Transaction B: Mechanical Engineering
Vol. 17, No. 6, pp. 480–491

Research Note

Experimental and Numerical Analysis of Turbulent Air Flow Around a Surface Mounted Hemisphere

M.M. Tavakol[1] and M. Yaghoubi[1,*]

Abstract. *The air flow field around a surface mounted hemisphere for different velocities is investigated experimentally and numerically. Hot-film anemometry is used in a wind tunnel to analyze the flow structure for different regions of flow domain around the hemisphere. The flow Reynolds number is varied based on the hemisphere diameter and free stream velocities. The air velocity is taken as 5, 7 and 8.5 m/s, with corresponding Reynolds numbers of 35000, 50000 and 64000. To illustrate the flow pattern around the hemisphere, variations of flow velocity at various vertical sections along the midplane, and cross-stream velocities for various surfaces and heights, are measured and plotted. Corresponding numerical solutions are also carried out to visualize the flow reversal, horseshoe vortices and recirculation zones around and downstream of the hemisphere. It is concluded that the flow is highly Reynolds number dependent, especially at the reversed flow region upstream and downstream of the hemisphere. Moreover, the effect of hemisphere location in the tunnel is studied, and velocity distributions are compared and presented in the wake of the hemisphere for constant free stream velocity.*

Keywords: *Hot-film anemometer; Reversed flow; Reynolds number; Wake structure; Turbulent flow.*

INTRODUCTION

Three-dimensional flow structures and separation bubbles formed around a wall mounted obstacle in turbulent boundary layers are important in many engineering applications. For example, transport phenomena, such as heat and mass transfer, aerodynamic loading and dispersion of dust and air suspended particles, are related to the structure of the flow field around different buildings. Additional complexity arises for curved bodies (e.g. hemisphere and cylinders) because the location of a separation point cannot be identified purely based on the geometry. This leads to a strong dependency of flow field on Reynolds number, boundary layer thickness and the turbulence intensity level of the approaching flow.

For such curved bodies, various experimental and numerical studies have been undertaken to determine flow structure and wind loads. The early work of Maher [1] was conducted for a Reynolds number of about 150,000 (based on the hemisphere diameter) in a thin boundary layer to find the pressure distribution on smooth and rough domes in a wind tunnel. Results show that the minimum mean pressure coefficients for smooth and rough domes are -1.15 and -0.8, respectively. Also, a reduction in the maximum pressure coefficient is occurred because the rough surface promotes the turbulent boundary layer over the dome and causes earlier separation over the dome. Consequently, the earlier separation over the dome reduced suction at the separation point, but led to more suction overall in the wake and increased drag. Other authors extended experiments for different boundary layers and different Reynolds numbers. Savory and Toy [2,3] undertook a series of investigations to find the velocity and pressure distribution around the hemisphere and hemisphere-cylinders for different incoming velocity and turbulence intensity boundary layer profiles. Acarlar and Smith [4] performed a flow visualization technique to investigate the role of different vortices formed in the flow field around a hemisphere mounted on a laminar boundary layer. Numerical studies provided some additional information about the structure of

1. *School of Mechanical Engineering, Shiraz University, Shiraz, P.O. Box 71348-51154, Iran.*
*. *Corresponding author. E-mail: yaghoubi@shirazu.ac.ir*

Received 7 February 2010; received in revised form 4 July 2010; accepted 14 August 2010

flow around hemispheres and domes. Suzuki et al. [5] described pressure fluctuations on the surface of a hemisphere in a thick turbulent boundary layer using wind tunnel measurements. Statistical properties of pressure data involving time mean, root mean square, probability density and the power spectrum of pressure fluctuations are presented. Tamura et al. [6] used numerical simulation to find the unsteady flow field around a wall mounted hemisphere. Manhart [7] carried out a large eddy simulation to investigate vortex shedding from a hemisphere in a turbulent boundary layer. Meroney [8] conducted numerical simulation, as well as wind tunnel measurements, to study flow around single and dual domes in a thick turbulent boundary layer. Lin and Zmeureanu [9] undertook thermal and air flow analysis to estimate the energy need of a domed-covered house. Transient three-dimensional thermal and air flow models have been performed by [9] to evaluate the impact of a large scale dome on the heating energy needs of a house built inside the dome. Results showed that a reduction of 62.6% of the annual heating load of a house was achieved when a dome protected house was used, compared with an unprotected house under Canadian climate conditions. Faghih and Bahadori [10] conducted a wind tunnel study to analyze pressure distribution over a 1/10 scale model of a dome with a hole at the apex, and open and closed apertures. Pressure distribution over the dome is measured and pressure coefficients are presented for a dome with open and closed windows. It is concluded that the maximum value of the pressure coefficient is occurred at the lowest point on the dome in a windward direction. The value of C_p at this point is 1 for both cases with open and closed windows (and holes). Moreover, the value of the minimum pressure coefficient is reported to occur near the apex in a windward direction when the windows and the hole at the apex are all closed.

Recently, the present authors [11] reported a flow regime around a wall mounted hemisphere placed in two different boundary layers (thin and thick) using numerical simulation and hot-film anemometry. Velocity distribution at different sections of the flow field, locations of flow separation and reattachment are measured with a hot-film anemometer. Also a numerical simulation using a RNG $k-\varepsilon$ turbulence model is employed and results are compared with the wind tunnel measurements. It is concluded that the hemisphere located in a thin boundary layer profile has a greater reattachment length downstream of the hemisphere and a closer separation point to the hemisphere apex.

The present study provides some excessive flow structures of separated shear layer formed around a hemisphere. This work concentrates on the Reynolds number dependency of the separation bubble in the near wake, as well as in downstream recirculation, and different flow characteristics, developing and developed boundary layer profiles of the flow field around a wall mounted hemisphere.

EXPERIMENTAL APPARATUS AND MEASUREMENT TECHNIQUE

Tests are conducted in a blowing-type subsonic wind tunnel located in the School of Mechanical Engineering at Shiraz University. The tunnel cross section is 46 cm $\times$ 46 cm, as the experiments performed by [12], but the test section length is increased to 326 cm, as described in [11]. The test section is placed in such a way as to produce different entrance boundary layer thicknesses. The free stream velocity in the test section is varied by a frequency inverter and is controlled during each experiment by a pitot tube. The blower can provide velocities from 1 m/s up to 25 m/s in the tunnel test section.

The experimental setup consisted of a smooth wall mounted hemisphere inside the test section. The hemisphere model has a diameter of 12 cm, which leads to, approximately, a blockage of 3% in the tunnel. The location of the model in the test section and the reference coordinate system are shown in Figure 1. The three-dimensional traversing system from Fara Sanjesh Saba Co. (FSS) is installed outside the tunnel and is used to move the probe in the test section [11]. This mechanism allows the positioning of the probe to be adjusted with an accuracy of 0.1 mm at different locations in the test section. The time-mean and fluctuating velocity of the air flow are measured by linearized constant temperature hot-wire (hot-film) anemometers using a Dantec split-fiber and a special dual sensor hot-film probe from FSS. Split-fiber probes have two parallel nickel films deposited on the same quartz fiber; 200 μm in diameter and 3 mm long as shown in Figure 2. The probe body is a 2.3 mm diameter ceramic tube, equipped with gold-plated connector pins that connect to the probe supports by means of plug-and-socket arrangements. The split-fiber sensors had the plane normal to the main flow and, thus, were able to detect the reversal of air flow locally. The dual sensor probe consisted of two inline hot-film sensors. It is equipped with a proper shield, based on Gunkel et al. [13], and is used beside the split-fiber sensor to check for the protection of measurement in the separation bubble from other velocity components.

The Flow-Ware software developed by FSS is used for data acquisition and to obtain various statistical flow properties. Calibration for each probe is made, respectively, in the tunnel using the Karman-vortex method. In this method, a thin cylinder is used to create regular vortices in the tunnel. Each sensor is

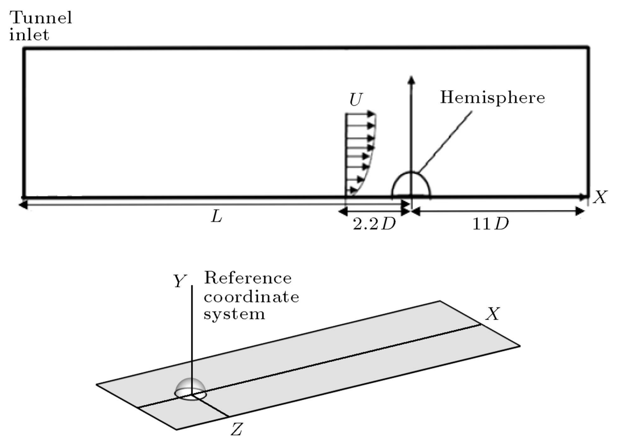

(a) Location of model in tunnel and reference coordinate system

(b) Wind tunnel with split-fiber probe and traversing system

Figure 1. Wind tunnel arrangement and measuring instrument.

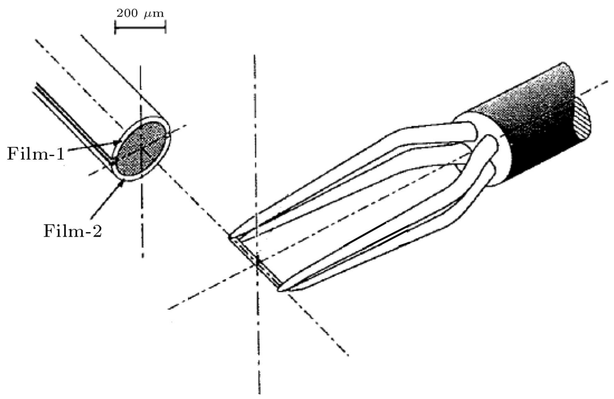

Figure 2. Tip of split fiber sensor.

placed at the proper distance from this cylinder, as shown in Figure 3, and then the calibration process is performed as described in [14,15].

Typical calibration curves for a split-fiber probe are shown in Figure 4. The advantage of this method, with respect to conventional pitot tube calibration, is for low velocity calibration (below 2 m/s) where the pressure difference is very small and it is difficult to measure air velocity accurately.

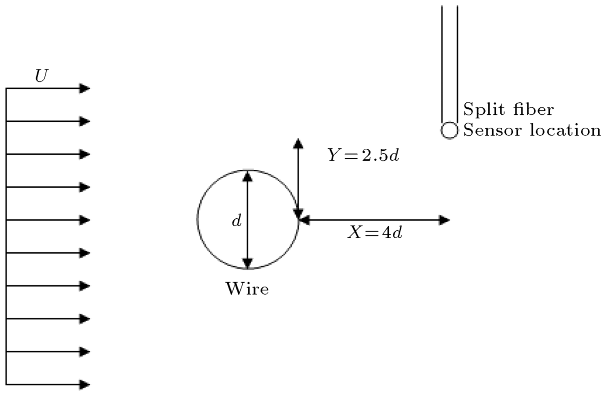

Figure 3. Schematic of wire cylinder and hot wire position for measuring frequency of vortex shedding.

RESULTS

Experimental Results

Figure 5 shows the inlet velocity profiles obtained from the hot-film anemometry measurements in the tunnel for three different air velocities. The free stream turbulence intensity is about 1% for various inlet air velocities. These profiles are measured at a distance of 2.2D upstream of the hemisphere center, as shown in Figure 5. To study the Reynolds number dependency of the flow field around the wall-mounted hemisphere, experiments are performed at different regions around the hemisphere. Hot-film anemometry is used to measure the streamwise velocity at different sections. Three lines at the plane of the symmetry of the hemisphere are selected and the velocity profiles are measured on these lines, as illustrated in Figure 6. The first line is selected upstream of the hemisphere. Based on the previous observations [11], two distinct reversed flow regions are formed in the flow field around the hemisphere. These regions are located upstream of the hemisphere due to boundary layer separation in front of the obstacle, and behind the hemisphere due to the separation of flow over the hemisphere. The second line is located over the hemisphere pick at plane of symmetry. The third line is selected behind the hemisphere where the recirculation zone forms and high velocity gradients are observed in the flow field.

Figure 6a shows the non-dimensional velocity profiles at plane $X/H = -1.17$ for three different free stream velocities where $X = 0$ is the center of the hemisphere. This figure supports the Reynolds number dependency of the flow field, especially at lower values of Reynolds number. Moreover, increasing the free stream velocity causes the reversed flow velocity upstream of the hemisphere to increase.

However, the recirculation region forms upstream of the hemisphere at plane of symmetry confined to a region near the wall, and it is substantially constant for different velocities.

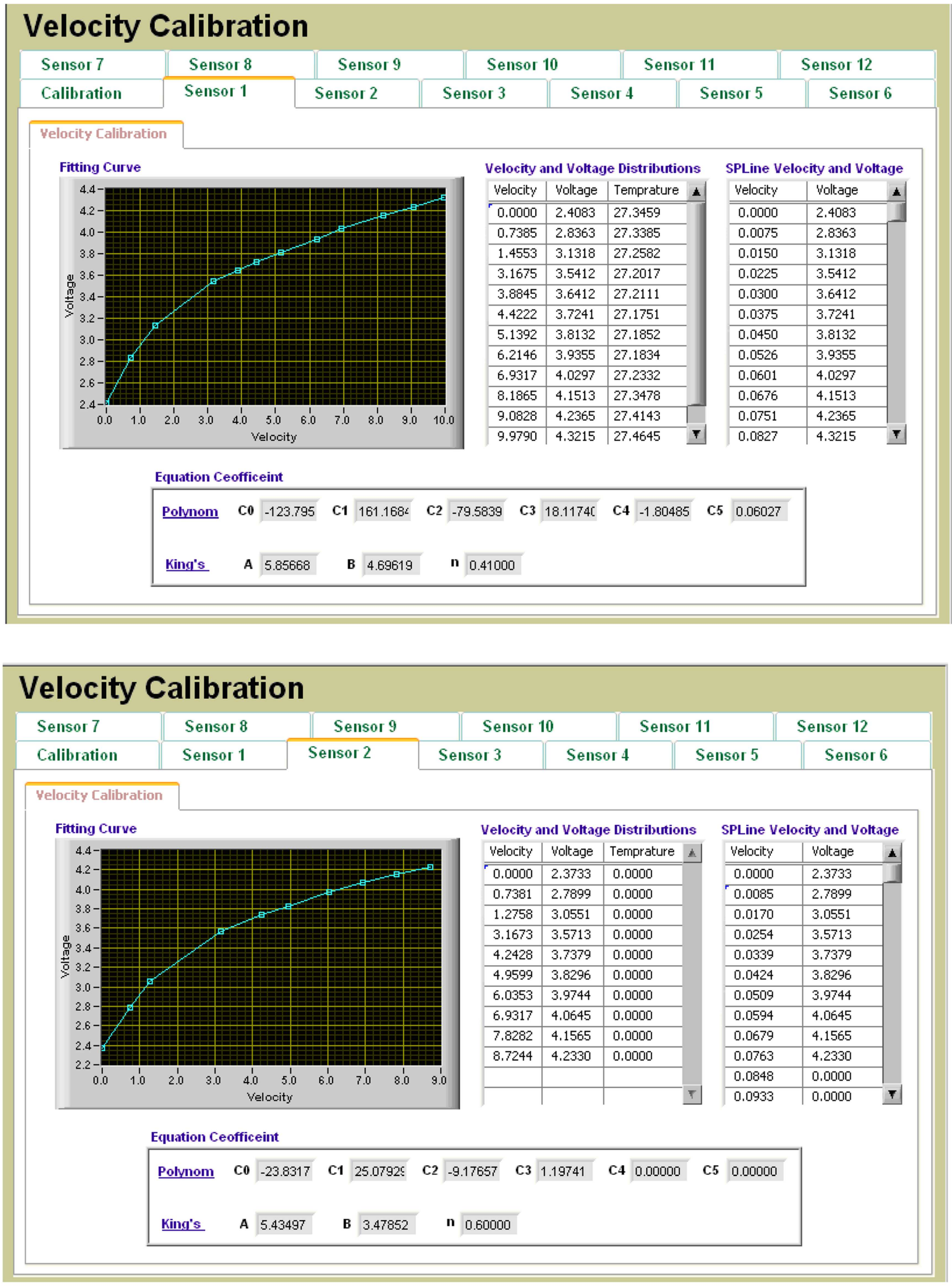

Figure 4. Calibration curves for split-fiber sensors.

Obviously, for $0.1 < Y/H < 0.5$ the flow is highly Reynolds number dependent and different blockage effects of the hemisphere are observed for this region. Figure 6b illustrates velocity profiles at plane $X/H = 0.0$ over the hemisphere. Flow accelerates over the dome due to the existence of a favorable pressure gradient and the maximum velocity is occurred at this region. A slight Reynolds number dependency is distinguished on this line and similar distribution can be observed for non-dimensional velocity profiles at this section. Also it is clear from Figure 6b that, at a height of $3H$, the air velocity matches the free stream velocity, and the hemisphere effect is diminished.

Velocity distribution for $X/H = 1.17$ at plane of

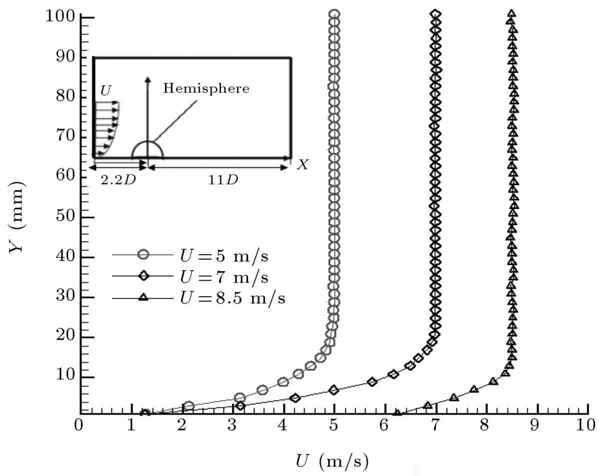

Figure 5. Inlet velocity profiles.

symmetry located in the wake region of the hemisphere is shown in Figure 6c. This figure shows that increasing the free stream velocity caused the reverse flow region to extend higher, but the maximum reversed flow velocity at this plane is decreased. Maximum values of non-dimensional streamwise velocity, u/U, at this line are: -0.4, -0.3 and -0.2 for free stream velocities of 5, 7 and 8.5 m/s, respectively.

Also Figure 6c illustrates a strong Reynolds number dependency on this plane, similar to the cavity zone upstream of the hemisphere. The velocity distributions in the spanwise direction downstream of the hemisphere at two different locations are presented and compared in Figure 7.

These velocity distributions are useful to evaluate the nature of flow at the wake region and reveal the spanwise extension of the shear layer around the hemisphere. Figure 7 depicts that increasing the streamwise distance from the hemisphere caused the recirculating zone to move toward the hemisphere. On the plane, $X/H = 1.34$, the velocity distribution shows that the separated shear layer extends to $Z/H = -1.3$ for different free stream velocities. At this plane, the sharper velocity distribution exists for the lower free stream velocities, and as the approaching velocity increased, the maximum velocity gradient and velocity decreased. Similar behavior is distinguished for the velocity distribution at plane $X/H = 1.67$. It should be noted that measurements are made on a half plane, and due to symmetry, the measurements are mirrored on the other half plane. Also, during hot-film measurements, no velocity fluctuation or unsteady behavior is detected. All experiments in the spanwise direction are undertaken using a shielded dual sensor probe to ensure the protection of measurements from the lateral velocity components.

The next analysis considers the effect of hemisphere location on the wake flow characteristics. In order to study it, the location of the hemisphere from

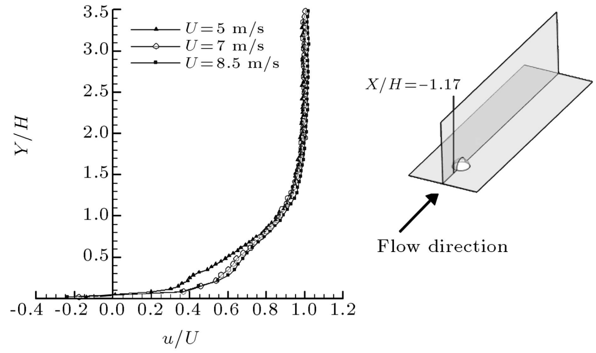

(a) $X/H = -1.17$

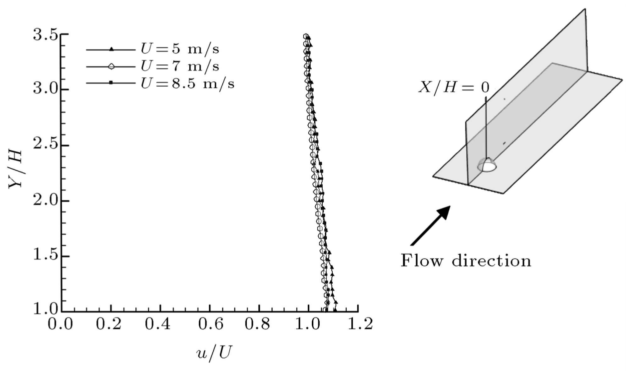

(b) $X/H = 0$

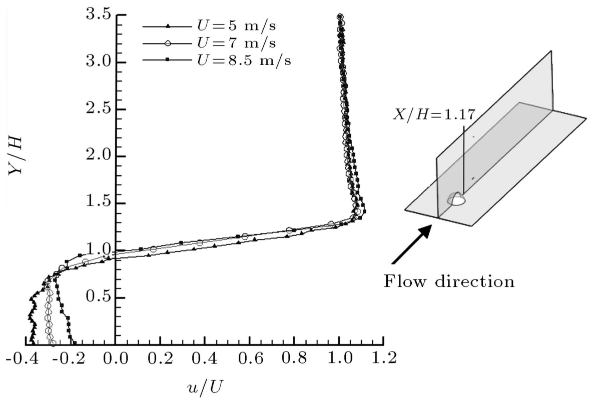

(c) $X/H = 1.17$

Figure 6. Non dimensional streamwise velocity at plane of symmetry for three different free stream velocities at different locations.

the tunnel inlet is changed and the velocity distribution is measured at different heights in a spanwise direction for the free stream velocity of 7 m/s. Figure 8 demonstrates the streamwise velocity in a spanwise direction at planes $X/H = 1.34$, $X/H = 1.67$ and $X/H = 2$ for the hemisphere located at $L = 4.2D$. It is clear that increasing the streamwise distance from the hemisphere caused the velocity distribution to change more with height. For $X/H = 1.34$, the velocity distribution is a weak function of height and possesses a high velocity gradient to reach the free stream velocity at upper

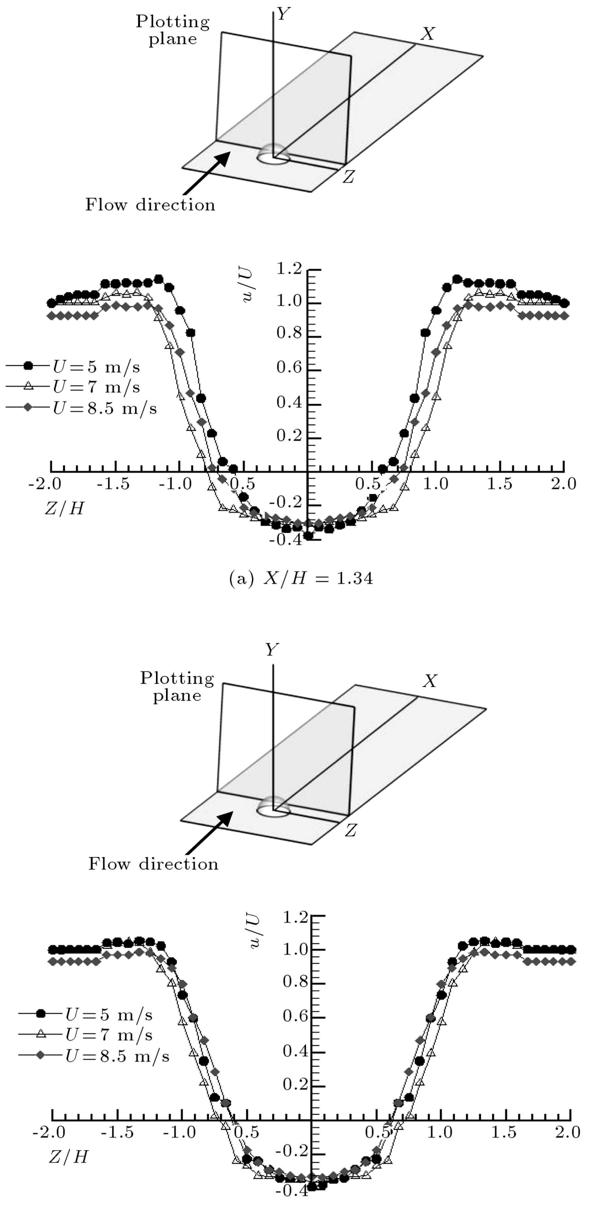

Figure 7. Spanwise velocity distribution at two locations behind the hemisphere for three different free stream velocities, $Y/H = 0.5$, $L = 4.2D$.

heights. This is due to the strong three dimensional separation from the hemisphere in a thin boundary layer profile, as previously reported by Savory and Toy [3] and Tavakol et al. [11]. At $Z/H > 1.5$ and $Z/H < -1.5$, as the height increases, the boundary layer profiles are observed and the velocity distribution in a spanwise direction reaches gradually to the free stream velocity. The reversed flow region behind the hemisphere extends to a maximum distance of 0.8 H at $X/H = 1.34$ for the region considered, and it is decreased by increasing height.

Figure 9 presents velocity distribution at $X/H = 1.34$, $X/H = 1.67$ and $X/H = 2$ for a hemisphere

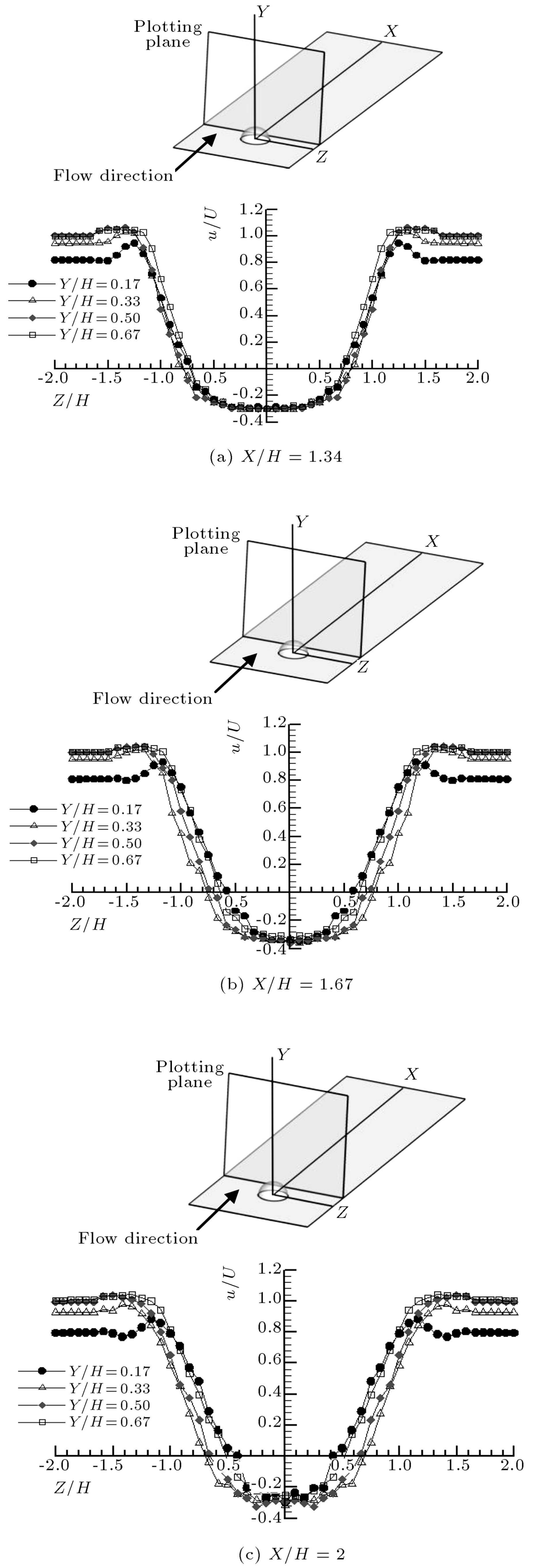

Figure 8. Spanwise velocity distribution for various locations behind the hemisphere for $U = 7$ m/s, $L = 4.2D$.

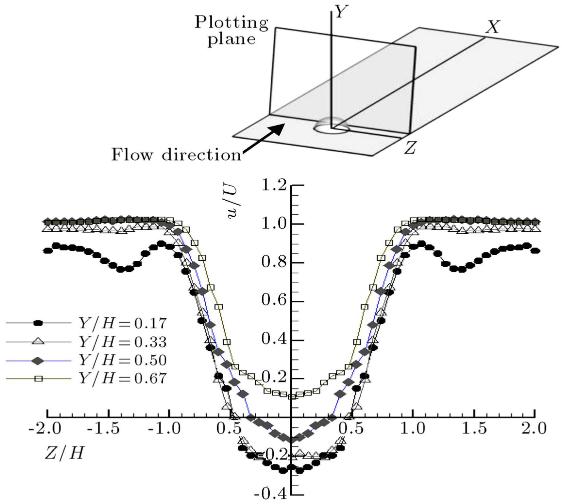

(a) $X/H = 1.34$

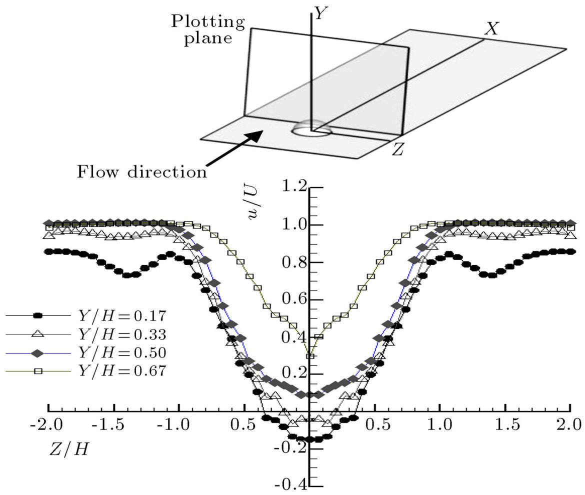

(b) $X/H = 1.67$

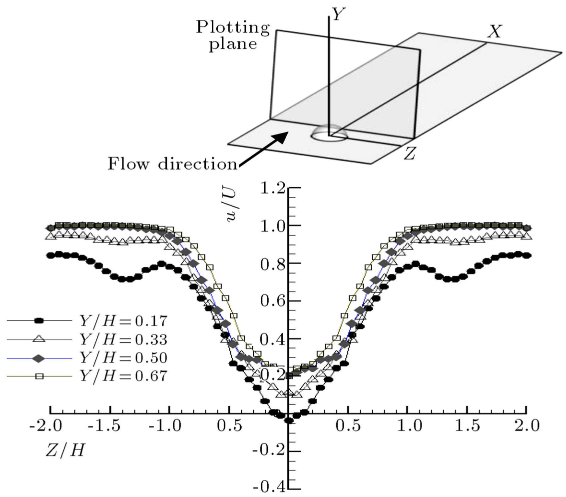

(c) $X/H = 2$

Figure 9. Spanwise velocity distribution for various locations behind the hemisphere for $U = 7$ m/s, $L = 12D$.

located at $L = 12D$. In this case, different spanwise velocity distributions in the wake region behind the hemisphere are observed, compared with Figure 8 of $L = 4.2D$. The width of the reversed flow region is restricted to the region near the hemisphere in comparison with the hemisphere located at $L = 4.2D$.

Moreover, velocity distribution at different distances from the hemisphere is changed rapidly in the vertical direction and the smaller cavity region formed around the hemisphere in Figure 9. The more developed boundary layer flow at a further distance from the tunnel inlet leads to a smaller cavity region behind the hemisphere in comparison with the developing boundary layer. In the previous study [11], similar observations are illustrated by changing boundary layer thickness. The reattachment length behind the hemisphere depends strongly on the incoming flow condition, i.e. free stream velocity and level of turbulence intensity. The experimental results of the present study show that the reattachment length behind the hemisphere is decreased with increasing free stream velocity. Another interesting observation is the velocity distribution at $Y/H = 0.17$ where the velocity profile is first decreased and then approached to the undisturbed velocity at the same height. For $L = 12D$, although the flow reversal diminished for $X/H > 2$, which is different from $L = 4.2D$ (Figure 8), the spanwise variation at $Z/H = 1.3$ remained the same.

Numerical Result

Numerical simulation is performed using a discretized code to study the flow field and pressure distribution around the wall mounted hemisphere in more detail; the numerical simulation being related to the first case where the hemisphere is located at $L = 4.2D$. The RNG $k - \varepsilon$ turbulence model, which has better prediction for flows with streamline curvature, is used for the numerical computation of the turbulent flow field around the hemisphere [16]. More details of the computational procedure and accuracy of the turbulence model are reported by [11,16]. The velocity profile obtained from the hot-film measurement in the tunnel shown in Figure 5 is used as the velocity inlet boundary condition for the computational domain.

The solution procedure and other boundary conditions are similar to the previous study [11] and these are not repeated here. Figure 10 depicts typical pathlines on the plane of symmetry obtained from the numerical simulation for different free stream velocities. Results are compared with the wind tunnel study of Savory and Toy [3]. Good agreement is observed for the flow patterns in this study and with the previous experimental measurements. Results of the present study show the formation of a horseshoe vortex

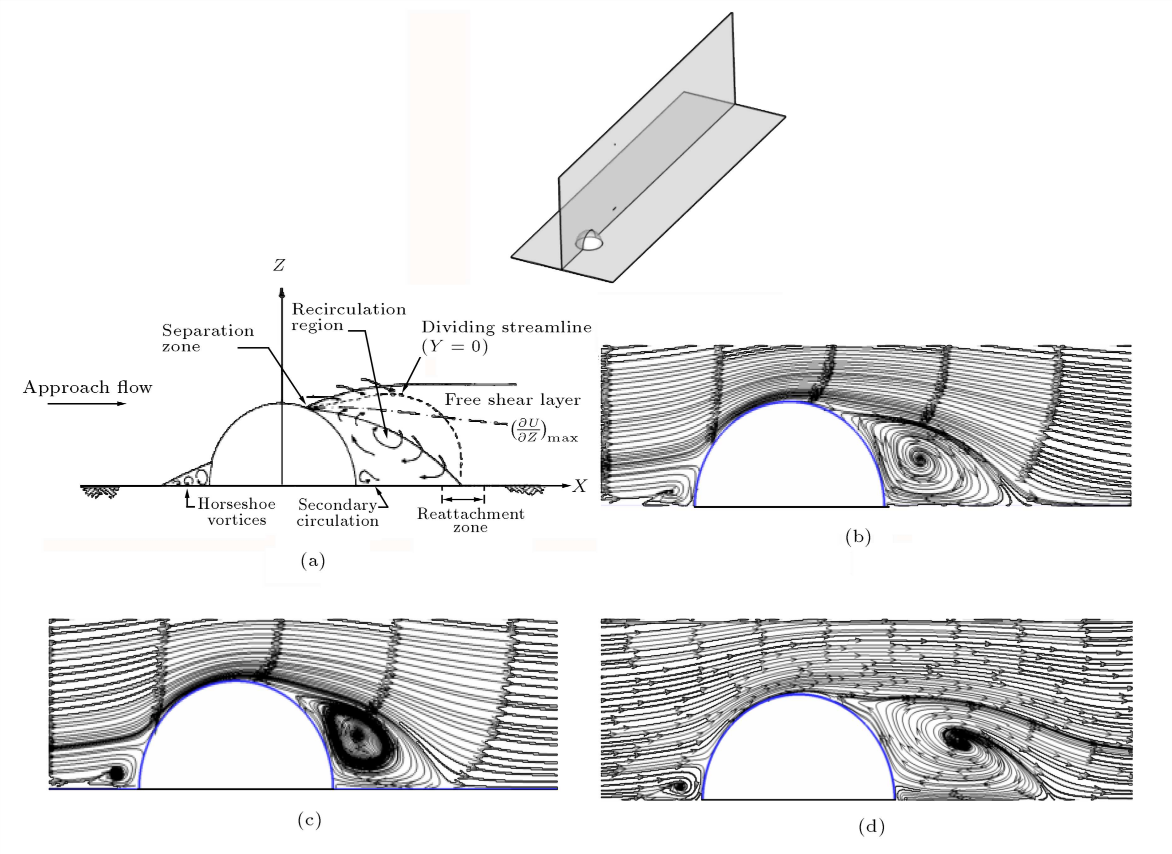

Figure 10. Typical pathlines on streamwise plane of symmetry for $L = 4.2D$. a) Experiment [3]; b) $U = 5$ m/s; c) $U = 7$ m/s; d) $U = 8.5$ m/s.

upstream of the hemisphere, flow separation over the hemisphere, formation of a recirculation zone behind the hemisphere and flow reattachment downstream of the hemisphere, similar to the experimental results. It is clear, in Figure 10, that the turbulence model captured the secondary circulation occurred at the hemisphere-wall junction behind the hemisphere and forward section. Figure 11 presents the pathlines at plane $Y/H = 0.17$ for three different free stream velocities. Again flow patterns obtained from the numerical simulation are compared with experimental results of Savory and Toy [3]. Similar to the plane of symmetry, the formation of a horseshoe vortex around the hemisphere that extends to the hemisphere far wake can be distinguished similar to experimental observation.

Figure 12 shows the isosurface of $u = 0$ around the hemisphere in comparison with the large eddy simulation of Manhart [7]. This figure shows that the recirculation zone behind the hemisphere is surrounded by the curve shear layer where the maximum value of turbulence intensity occurs near the edge of the shear layer [7,11]. Two distinct recirculation zones can be seen around the hemisphere similar to Figure 10. The first region is related to the horseshoe vortex in front of the hemisphere and the second region is formed due to the separation of flow over the back sides of the hemisphere. However, some differences between RNG $k - \varepsilon$ and LES predictions, especially in the wake region, are observable. It should be noted that LES is more preferable to the RNG $k - \varepsilon$ scheme for such highly complex flow structures downstream of the hemisphere.

Figure 13 depicts isosurfaces of $v = 0.5$ m/s and $v = -0.5$ m/s around the hemisphere. This figure clearly shows the region of positive and negative, v velocity around the hemisphere. In front of the hemisphere, the horseshoe vortex caused to the formation of a negative, v velocity region near the wall, which wraps around and extends downstream of the hemisphere. Except the small, negative, v velocity region, the positive, v velocity region is observed in front of the hemisphere. Conversely, behind the hemisphere, the negative, v velocity region is dominant due to strong suction induced from the recirculating zone behind the hemisphere.

Comparison between numerical and experimental results of streamwise velocity profiles are presented in Figure 14. Two lines at the plane of symmetry are selected and the results of the numerical simulation

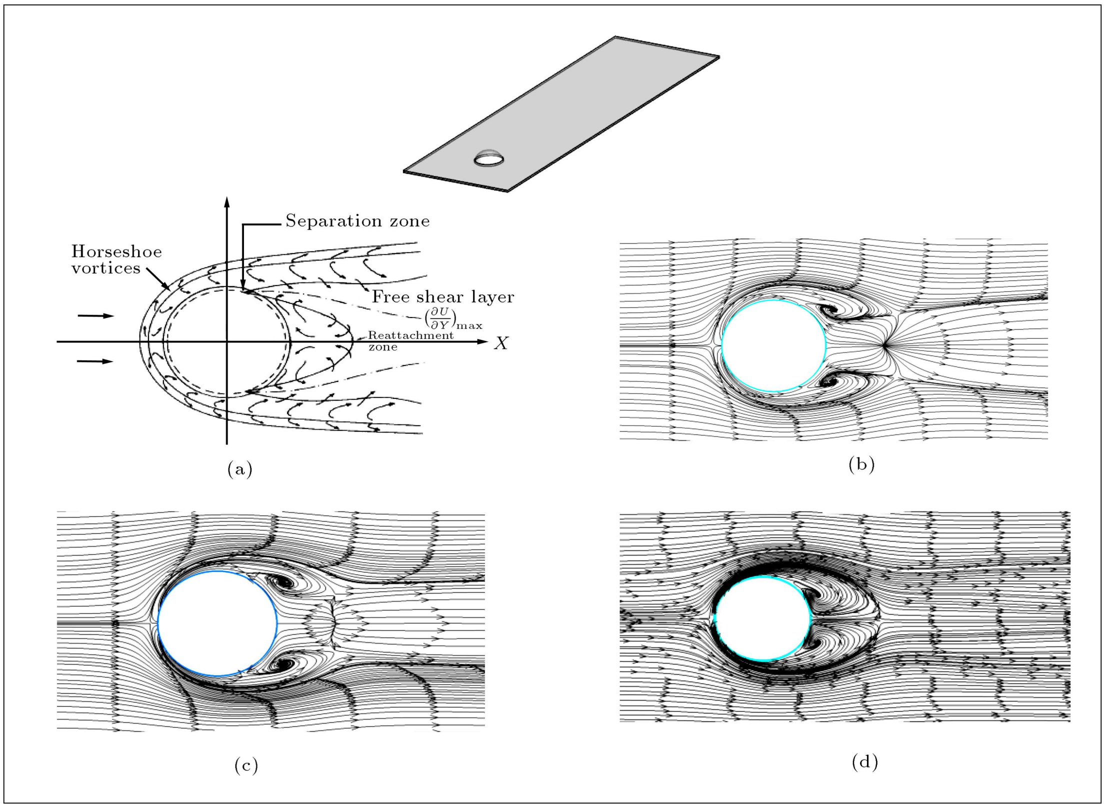

Figure 11. Typical pathlines on streamwise plane $Y/H = 0.17$ for $L = 4.2D$. a) Experiment [3]; b) $U = 5$ m/s; c) $U = 7$ m/s; d) $U = 8.5$ m/s.

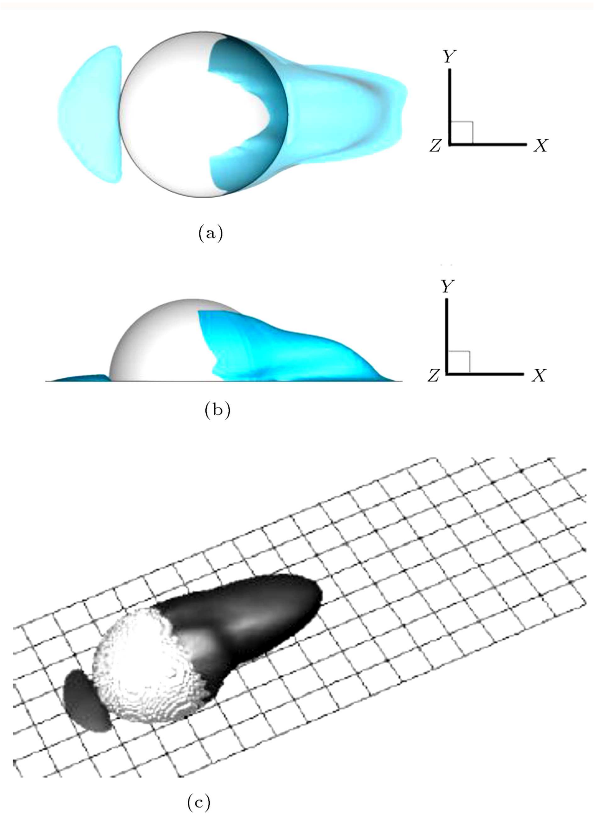

Figure 12. Isosurface of $u = 0$ for $U = 8.5$ m/s. a) Plan view; b) side view; c) LES [7].

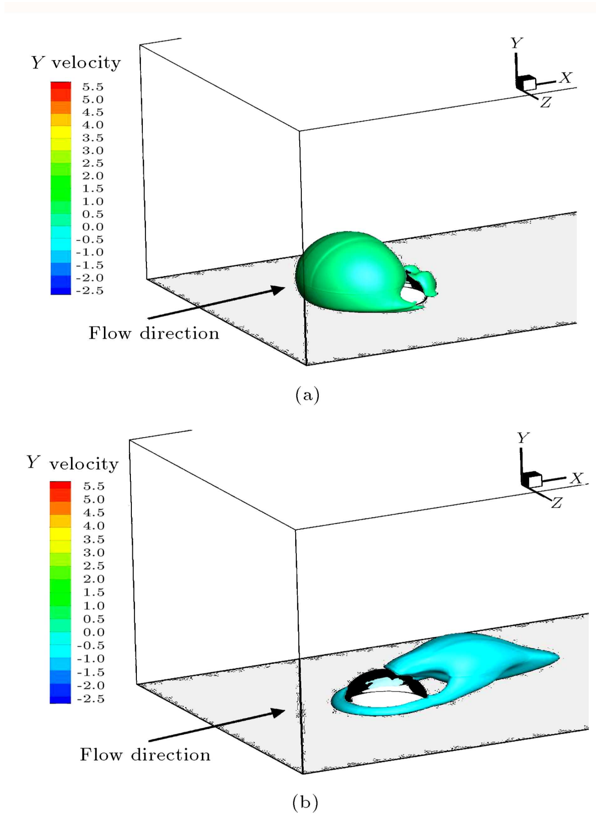

Figure 13. Isosurface of v velocity for $U = 8.5$ m/s. a) $v = 0.5$ m/s; b) $v = -0.5$ m/s.

are compared with the wind tunnel measurements. Good agreement is observed between the numerical and experimental results at plane $X/H = -1.17$ for different velocities, but at the plane of $X/H = 0$, some discrepancies of the numerical predictions are observed.

The turbulence model of RNG $k - \varepsilon$ overpredicts the streamwise velocity over the hemisphere for the lower free stream velocities. Such differences are mainly due to the turbulence model, which is not able to accurately predict the flows near the surface where

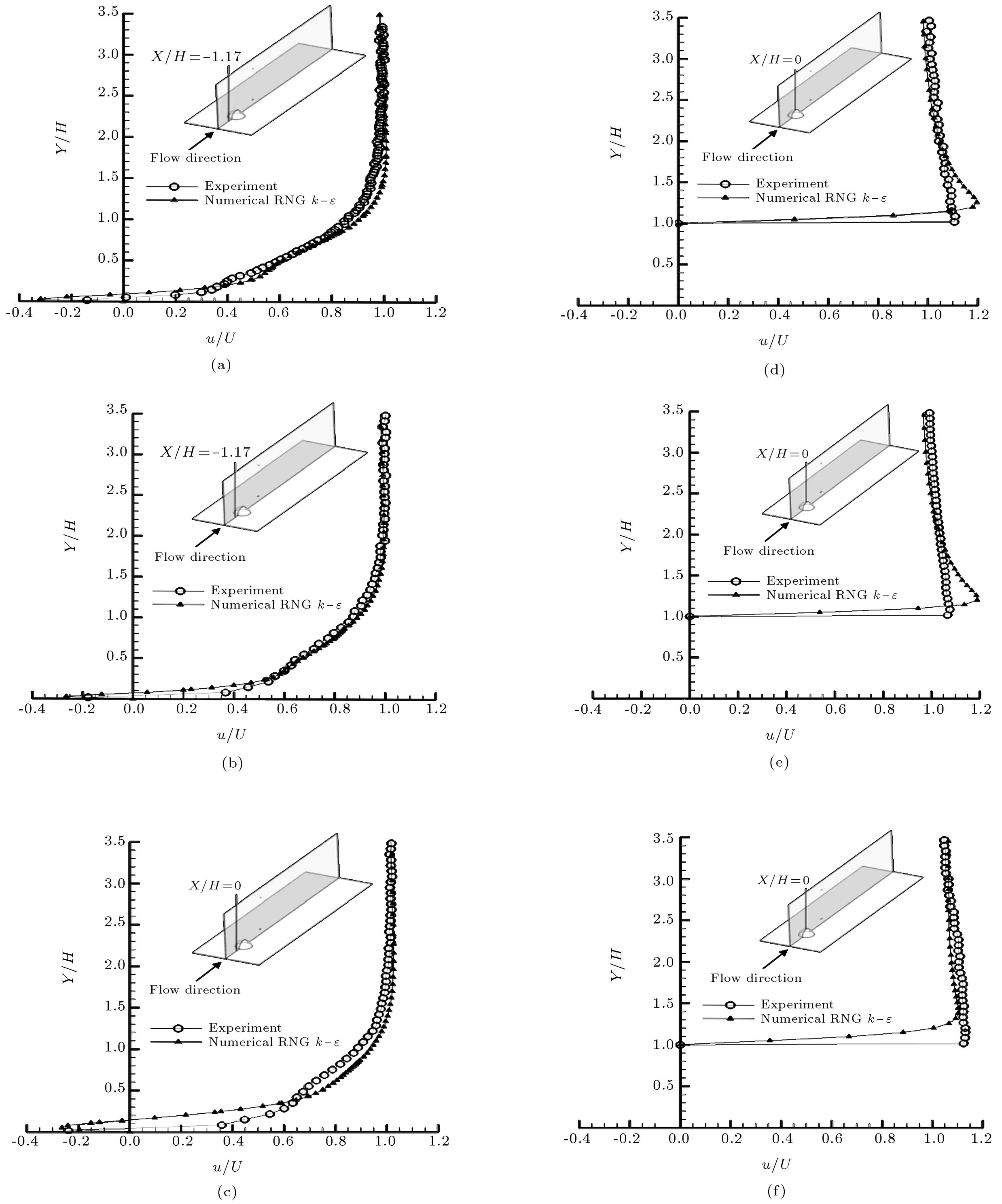

Figure 14. Comparison between experimental and numerical streamwise velocity at two sections in plane of symmetry. a) $U = 5$ m/s, $X/H = -1.17$; b) $U = 7$ m/s, $X/H = -1.17$; c) $U = 8.5$ m/s, $X/H = -1.17$; d) $U = 5$ m/s, $X/H = 0$; e) $U = 7$ m/s, $X/H = 0$; f) $U = 8.5$ m/s, $X/H = 0$.

grid Reynolds numbers are low and surface curvature is high. Such differences are also discussed in [11]. Behind the hemisphere, the numerical results for the streamwise velocity are in poor agreement with the experimental data. It is due to the formation of a complex flow field in the wake of the hemisphere by means of interference between the horseshoe vortex with the arc type vortices behind the hemisphere, and the vortex shedding process behind the hemisphere. More accurate numerical simulation like Large Eddy Simulation, as emphasized in [17], should be performed to have a more accurate reading of the flow field in this region.

CONCLUSIONS

From flow measurements in the wake of a surface mounted hemisphere in a turbulent boundary layer and a corresponding numerical simulation, the following conclusions are made:

1. The flow is highly Reynolds number dependent, especially at the reversed flow region formed upstream and downstream of the hemisphere.
2. The maximum value of reversed velocity at the upstream zone of the hemisphere is observed for lower air velocity, i.e. $U = 5$ m/s, due to a stronger blockage in the flow field.
3. Conversely, as the velocity increased downstream of the hemisphere, the maximum reversed velocity is decreased and the maximum value is related to the higher free stream velocity of $U = 8.5$ m/s.
4. For a spanwise direction, the maximum reversed flow occurs for the lower free stream velocity of $U = 5$ m/s.
5. Velocity profiles changed rapidly with height in the spanwise direction, where the hemisphere is moved to a further distance from the tunnel inlet.
6. The incoming boundary layer flow has a strong effect on the flow pattern around the hemisphere in the subcritical regime. The sizes of the recirculation zone in front of the hemisphere and the cavity region behind the hemisphere are changed for different approaching free stream velocities.

ACKNOWLEDGMENT

This work is supported by Shiraz University, Grant number No. 88-GR-ENG-45 and the Academy of Science I.R. IRAN. Also the authors acknowledge Engineer Azodi, Dr. Ardekani and Engineer Masoudi (FSS) for providing the experimental facilities. The numerical simulations were performed at the high performance computer center of the School of Mechanical Engineering at Shiraz University.

NOMENCLATURE

d	wire diameter
D	hemisphere diameter
f	vortex shedding frequency
H	hemisphere height
Re_H	Reynolds number based on hemisphere height
S_N	Strouhal number
U	free stream velocity
u/U	dimensionless streamwise velocity
v	normal velocity
X	streamwise direction
X/D	dimensionless streamwise distance based on D
X/H	dimensionless streamwise distance based on H
Y/H	dimensionless normal distance based on H
Y	vertical direction
Z/H	dimensionless spanwise distance based on H
Z	spanwise direction

REFERENCES

1. Maher, F.J. "Wind loads on basic dome shapes", *J. Structural Division.*, **91**, pp. 219-228 (1965).
2. Savory, E. and Toy, N. "Hemisphere and hemisphere-cylinders in turbulent boundary layers", *J. Wind Eng. and Ind. Aero.*, **23**, pp. 345-364 (1986).
3. Savory, E. and Toy, N. "The separated shear layers associated with hemispherical bodies in turbulent boundary layers", *J. Wind Eng. Industrial Aerodynamics*, **28**, pp. 291-300 (1988).
4. Acarlar, M.S. and Smith, C.R. "A study of hairpin vortices in a laminar boundary. Part 1. Hairpin vortices generated by a hemisphere protuberance", *J. Fluid Mech.*, **175**, pp. 1-41 (1987).
5. Suzuki, Y., Kiya, M., Sampo, T. and Naka, T. "Pressure fluctuations on the surface of a hemisphere immersed in thick turbulent boundary layer", *J. Fluids Eng.*, **109**, pp. 130-135 (1987).
6. Tamura, T., Kuwahara, K. and Suzuki, M. "Numerical study of wind pressures on a domed roof and near wake flows", *J. Wind Eng. and Ind. Aero.*, **36**, pp. 1001-1010 (1990).
7. Manhart, M. "Vortex shedding from a hemisphere in a turbulence in a turbulent boundary layer", *J. Theoretical and Computational Fluid Dynamics*, **40**, pp. 199-213 (1991).
8. Meroney, R.N., Letchford, C.W. and Sarkar, P.P. "Comparison of numerical and wind tunnel simulation

of wind loads on smooth, rough and dual domes immersed in a boundary layer", *J. Wind and Structures*, **5**, pp. 347-358 (2002).

9. Lin, Y. and Zmeureanu, R. "Three-dimensional thermal and airflow (3D-TAF) model of a dome covered house in Canada", *Renewable Energy*, **33**, pp. 22-34 (2008).
10. Faghih, A.K. and Bahadori, M.N. "Experimental investigation of air flow over domed roofs", *Iranian Journal of Science and Technology, Transaction B, Engineering*, **33**, pp. 207-216 (2009).
11. Tavakol, M.M., Yaghoubi, M. and Masoudi Motlagh, M. "Air flow aerodynamic on a wall mounted hemisphere for various turbulent boundary layers", *Exp. Therm. Fluid. Sci.*, **34**, pp. 538-553 (2010).
12. Yaghoubi, M. and Mahmoodi, S. "Experimental study of turbulent separated and reattached flow over a finite blunt plate", *Experimental Thermal and Fluid Science*, **29**, pp. 105-112 (2004).
13. Gunkel, A.A., Patel, R.P. and Weber, M.E. "A shielded hot-wire probe for highly turbulent flows and rapidly reversing flows", *Ind. Eng. Chem. Fund.*, **10**, pp. 627-631 (1971).
14. Ardekani, M.A. "Hot-wire calibration using vortex shedding", *Measurement*, **42**, pp. 722-729 (2009).
15. Schilichting, H., *Boundary Layer Theory*, Springer (2000).
16. Shaeri, M.R. and Yaghoubi, M. "Numerical analysis of turbulent convection heat transfer from an array of perforated fins", *Int. J. of Heat and Fluid Flow.*, **30**, pp. 218-228 (2009).
17. Farhadi, M. and Rahnama, M. "Large eddy simulation of separated flow over a wall-mounted cube", *Scientia Iranica*, **13**(2), pp. 124-133 (2006).

BIOGRAPHIES

Mohammad Mehdi Tavakol was born in Shiraz in 1983. He received his B.S. and M.S. degrees in 2006 and 2009, respectively, from the Mechanical Engineering School of Shiraz University, Shiraz, Iran, where he is currently a Ph.D. student. His research is focused on the Experimental and Numerical Study of Turbulent Air Flow around Bluff Bodies, such as Curved Roof, Semi-Sphere, and Semi-Cylinders. He has published five articles in journals and conference proceedings.

Mahmood Yaghoubi is a Professor at the Mechanical Engineering School of Shiraz University. He obtained his B.S. and M.S. degrees from Shiraz University in 1971 and 1973, respectively, and his Ph.D. from the Mechanical Engineering School of Purdue University, USA in 1978. His research areas include Heat Transfer, Solar Thermal Power Plant, Computational Fluid Dynamics and Engineering Education. He is a Fellow of the Academy of Sciences I.R. Iran.